STRUCTURAL BIOLOGY

ISSN 2059-7983

Phosphatidylinositol transfer protein α binds microcolins in its open conformation

Andrea Eisenreichova,[a] Martin Klima,[a] Tamas Balla[b] and Evzen Boura[a]*

[a]Institute of Organic Chemistry and Biochemistry, Academy of Sciences of the Czech Republic, v.v.i., Flemingovo nam. 2, 166 10 Prague, Czech Republic, and [b]Section on Molecular Signal Transduction, Eunice Kennedy Shriver National Institute of Child Health and Human Development, National Institutes of Health, Bethesda, MD 20892, USA. *Correspondence e-mail: boura@uochb.cas.cz

Received 4 December 2025
Accepted 28 January 2026

Edited by M. Czjzek, Station Biologique de Roscoff, France

Keywords: lipid transport; crystal structure; inhibitors; PITPs.

PDB reference: PITPα, complex with microcolin H, 9ta5

Supporting information: this article has supporting information at journals.iucr.org/d

Phosphatidylinositol transfer proteins (PITPs) are essential lipid-binding proteins that regulate phosphoinositide signaling, membrane trafficking and autophagy through the transport of phosphatidylinositol and other phospholipids between intracellular membranes. Microcolin compounds have been identified as selective inhibitors of class I PITPs, revealing important roles of PITPs in Hippo signaling and autophagy. Here, we report the crystal structure of human PITPα in complex with microcolin H at 2.0 Å resolution. The structure enables a detailed description of the interaction between microcolin H and the lipid-binding cavity. Besides the expected covalent bond to the Cys94 residue, the structure also reveals an extensive network of hydrogen bonds, water bridges and hydrophobic interactions. Importantly, PITPα remains in the open conformation upon binding to microcolin H. Quantitative cavity analysis confirms that the microcolin-bound structure adopts a volume comparable to that of the unliganded PITPα and is markedly larger than that of the lipid-bound state. These findings demonstrate that microcolins selectively trap PITPα in an open conformation and provide a structural basis for their inhibitory mechanism. Furthermore, our results show that ligand binding can profoundly change protein conformation, which underscores the limitation of docking experiments.

1. Introduction

Phosphatidylinositol transfer proteins (PITPs) are small cytoplasmic proteins capable of transporting specific phospholipids, namely phosphatidylinositol (PI), phosphatidylcholine (PC) or phosphatidic acid (PA), between membranes of intracellular organelles. They were discovered in studies showing that soluble proteins can mediate the exchange of phospholipids between membranes (Wirtz & Zilversmit, 1969). Since these early studies, enormous progress has been made in revealing the structural and functional features of these proteins (reviewed in Ashlin *et al.*, 2021; Pathak *et al.*, 2024). PITPs belong to the Start domain family of lipid-transfer proteins and have been classified based on their molecular architecture and sequence homology (Fig. 1). There are two class I PITPs, PITPα and PITPβ, coded by two genes, PITPNA and PITPNB, with two splice forms of PITPβ. These are small soluble proteins of ∼32 kDa in size that are capable of transporting either PI or PC bound in their hydrophobic cavities. Class IIA PITPs, which include Nir2 and Nir3, encoded by the PITPNM1 and PITPNM2 genes, are larger, ∼120 kDa proteins that contain several additional domains besides their N-terminal PITP domains. These include an FFAT motif mediating interaction with ER-anchored VAP-A/B proteins, a DDHD domain that is also present in three

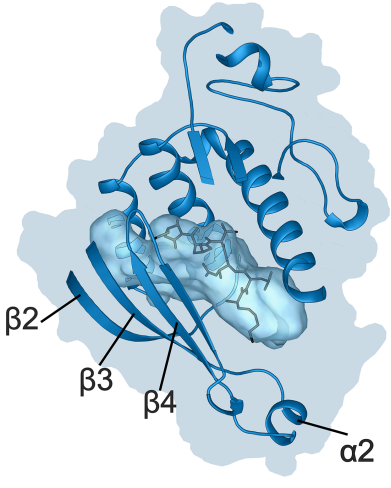

phospholipase A1 proteins (iPLA1α, iPLA1β and iPLA1γ, also named DDHD1, p125/Sec23IP and DDHD2, respectively) and an LNS2 domain at the C-terminus that mediates binding to PA (see Kim *et al.*, 2025; Raghu *et al.*, 2021). Class IIB is represented by RdgBβ, a smaller protein that shows the highest sequence homology to the PITP domains of Nir2 and Nir3 and is encoded by the PITPNC1 gene expressed in two splice forms. Unlike the class I PITPs that bind PI and PC, class II PITPs can bind and transport PI and PA instead (Garner *et al.*, 2012).

While many studies have explored and characterized the functions and properties of these proteins (reviewed in Ashlin *et al.*, 2021; Grabon *et al.*, 2019; Pathak *et al.*, 2024), the recent identification of microcolin compounds as specific inhibitors of class I PITPs has greatly facilitated the understanding of their functions and revealed their unique importance in Hippo signaling and autophagy (Li *et al.*, 2022; Yang *et al.*, 2023). In our recent studies we have reported the structure of PITPα in complex with one of these compounds, VT01454, a synthetic derivative of microcolin B, with improved potency against class I PITPs (Kim *et al.*, 2024). In another recent report, molecular docking through a computational approach was used to predict the structure of PITPα in complex with various microcolins, including microcolin H (Bailly & Vergoten, 2025). In the present study, we report the X-ray structure of PITPα in complex with microcolin H and discuss the implications of its structural features as they relate to the lipid-transport function of these proteins.

2. Materials and methods

2.1. Protein expression and purification

The recombinant PITPα protein was expressed as described previously (Kim *et al.*, 2024) using our standard protocols for lipid-binding/transport proteins (Eisenreichova, Humpolickova *et al.*, 2023; Eisenreichova, Klima *et al.*, 2023). Briefly, PITPα was expressed with an N-terminal 6×His tag followed by a SUMO tag. The construct was expressed in *Escherichia coli* BL21 Star cells, which were induced with 300 µ*M* isopropyl β-D-1-thiogalactopyranoside upon reaching an OD_{600} of 0.7. After overnight incubation at 18°C, the cells were harvested, resuspended in wash buffer (50 m*M* Tris pH 8.0, 300 m*M* NaCl, 10% glycerol, 20 m*M* imidazole, 3 m*M* 2-mercaptoethanol) and lysed by sonication. The clarified lysate was loaded onto Ni–NTA resin and incubated for one hour. Following several washing rounds with wash buffer, the protein was eluted with elution buffer (50 m*M* Tris pH 8.0, 300 m*M* NaCl, 10% glycerol, 300 m*M* imidazole, 3 m*M* 2-mercaptoethanol). The His_6–SUMO tag was removed by overnight Ulp1 protease digestion (4°C). The protein was subsequently purified by anion-exchange chromatography on a HiTrap Q HP column (Cytiva) in 20 m*M* Tris pH 8.0 using a NaCl gradient, followed by size-exclusion chromatography on a HiLoad 16/600 Superdex 75 pg column (Cytiva) equilibrated in 20 m*M* Tris pH 7.4. The purified protein was concentrated to 12 mg ml^{-1} and stored at −80°C.

2.2. Crystallization and crystallographic analysis

For crystallographic analysis, the protein was mixed with microcolin H (MedChemExpress) at a molar ratio of 1:1.5 (protein:inhibitor) and incubated at room temperature for approximately one hour. Crystallization trials were set up using the sitting-drop vapor-diffusion method. Each drop consisted of 150 nl protein–ligand mixture and 150 nl reservoir solution from various commercial screening kits, dispensed using a Mosquito robot (SPT Labtech). Crystals appeared after a week in multiple conditions. However, only crystals from condition C7 of the JCSG IV screen [0.1 *M* imidazole pH 8, 10%(*w*/*v*) PEG 8000] achieved diffraction quality. These crystals were transferred into the reservoir solution supplemented with 20% glycerol for cryoprotection and then flash-cooled in liquid nitrogen.

The crystallographic data set was collected from a single crystal on the BL14.1 beamline at the BESSY II electron-storage ring operated by the Helmholtz-Zentrum Berlin (Mueller *et al.*, 2025). The data were processed using *XDS* (Kabsch, 2010; Sparta *et al.*, 2016). The structure of PITPα covalently bound to microcolin H was solved by molecular replacement using the structure of PITPα in complex with the inhibitor VT01545 as a search model (PDB entry 8pqo; Kim *et al.*, 2024) in the program *Phaser* v.2.8.3 (McCoy *et al.*, 2007). The obtained initial model was further improved using automatic model refinement with the *phenix.refine* tool (Afonine *et al.*, 2012) from the *Phenix* package v.1.20.1-4487 (Liebschner *et al.*, 2019) and manual model building with *Coot* v.0.9.8.7 (Emsley *et al.*, 2010). Geometrical restraints for the cysteine residue covalently linked to microcolin H were generated with *Grade*2 v.1.7.1 (Global Phasing). Statistics for data collection and processing, structure solution and refinement are summarized in Table 1. Structural figures were generated with the *PyMOL* molecular-graphics system v.2.5.4 (Schrödinger). The finalized coordinates and structure factors have been deposited in the Protein Data Bank (https://www.rcsb.org) under accession code 9ta5. To calculate the cavities presented in Fig. 3, the *CavitOmiX PyMOL* plugin (v.1.0; Innophore) was used with its default settings except for the following: the grid spacing was set to 1, the probe radius to 2 and the softness to 1.3.

3. Results and discussion

3.1. PITPα–microcolin H complex at atomic resolution

Recent studies revealed that microcolin drugs bind class I PITPs (Pathak *et al.*, 2024; Yang *et al.*, 2023; Zhang, 2025). Here, we selected microcolin H for structural analysis because it was recently identified as an autophagy inducer with anti-tumor potential, specifically causing autophagic cell death in tumors (Yang *et al.*, 2023). Furthermore, a recent docking study suggested that microcolin H binds to PITP with the highest *in silico* affinity among all microcolins tested (Bailly & Vergoten, 2025).

To obtain the crystal structure of PITPα bound to microcolin H, purified recombinant PITPα was incubated with the

Table 1
Data-collection and processing, structure-solution and refinement statistics for the crystal structure of PITPα covalently bound to microcolin H (PDB entry 9ta5).

Values in parentheses are for the highest resolution shell. R.m.s.d., root-mean-square deviation.

Data collection and processing	
Space group	$P2_12_12$
a, *b*, *c* (Å)	82.2, 94.5, 50.7
α, β, γ (°)	90.0, 90.0, 90.0
Resolution range (Å)	44.64–2.10 (2.18–2.10)
No. of unique reflections	23316 (2309)
Completeness (%)	94.5 (100.0)
Multiplicity	12.4 (13.6)
Mean $I/\sigma(I)$	12.13 (0.96)
Wilson *B* factor (Å^2)	38.47
R_{merge}	0.1849 (2.874)
R_{meas}	0.1933 (2.986)
$CC_{1/2}$ (%)	99.8 (51.1)
CC* (%)	99.9 (82.2)
Structure solution and refinement	
R_{work} (%)	24.87 (37.58)
R_{free} (%)	26.32 (41.86)
CC_{work} (%)	89.4 (73.0)
CC_{free} (%)	92.6 (67.6)
R.m.s.d., bond lengths (Å)	0.002
R.m.s.d., angles (°)	0.52
Average *B* factor (Å^2)	
Overall	50.98
Protein	51.60
Ligands	42.67
Solvent	43.66
Clashscore	0.96
Ramachandran statistics (%)	
Favored	99.6
Allowed	0.4
Outliers	0.0

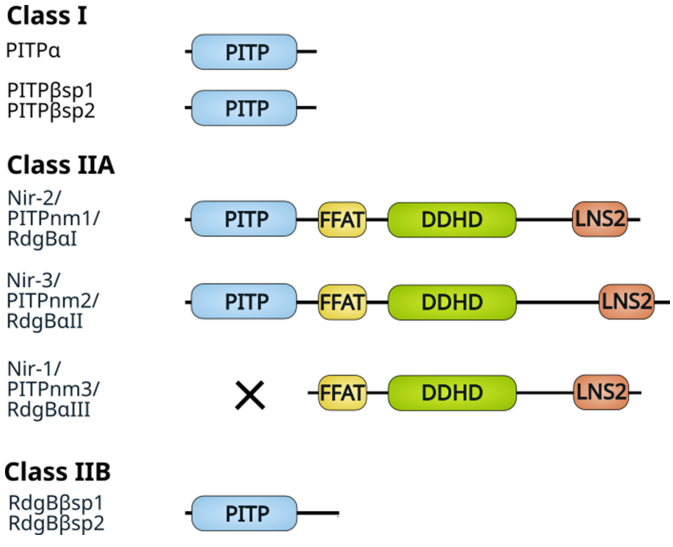

Figure 1
Domain organization of phosphatidylinositol transfer proteins (PITPs). Schematic representation of the domain architecture of PITP family members classified into class I, class IIA and class IIB. Class I proteins (PITPα and PITPβ splice variants) consist solely of the PITP domain. Class IIA proteins (Nir2/PITPNM1/RdgBαI and Nir3/PITPNM2/RdgBαII) contain an N-terminal PITP domain followed by an FFAT motif, a central DDHD domain and a C-terminal LNS2 domain. Nir1/PITPNM3/RdgBαIII lacks the N-terminal PITP domain but retains the FFAT, DDHD and LNS2 domains. Class IIB proteins (RdgBβ splice variants) consist only of the PITP domain.

compound in a 1.5-fold molar excess. Because microcolins bind irreversibly to a conserved cysteine residue (Cys94) in the center of the cavity (Li *et al.*, 2022), the mixture was incubated at room temperature for one hour prior to crystallization screening. Crystals formed under multiple conditions; however, diffraction-quality crystals were only obtained from a single condition (see Section 2). These crystals diffracted to approximately 2 Å resolution and belonged to the orthorhombic space group $P2_12_12_1$. The structure was solved by molecular replacement using the PITPα–VT01454 complex (PDB entry 8pqo) as the search model.

Immediately after molecular replacement, clear electron density corresponding to microcolin H was visible (Fig. 2*a*). The structure was refined to good geometry and *R* factors, as detailed in Section 2 and Table 1. The high resolution allowed us to directly observe the binding of microcolin H to PITPα (Fig. 2*b*).

The defining feature of this structure is a covalent bond that is formed between microcolin H and Cys94, which provides the anchoring point for microcolin H within the binding cavity. This bond is formed by the addition of the cysteine thiol group to the conjugated double bond of the ligand. In principle, this represents a nucleophilic conjugate (Michael) addition. Surrounding this covalent attachment, Gln22 and Lys194 form direct hydrogen bonds to microcolin O atoms. Other residues, including Tyr18, Thr113, His115 and Glu217, form water bridges with the ligand. In addition to these polar contacts, the hydrophobic region of the cavity, physiologically occupied by the acyl chains of the lipid ligands, stabilizes microcolin H through an array of hydrophobic interactions; specifically, with Ile83, Ile98, Phe107, Ile109, Phe221 and Phe224, which promote deep burial of the ligand through nonpolar packing. Together, these covalent, hydrogen-bonding, water-mediated and hydrophobic interactions define a tightly integrated binding interface between PITPα and microcolin H (Fig. 2*b*).

3.2. PITPα binds microcolin H in its open conformation

Structural studies have shown that PITPα can adopt two basic conformations, open and closed, which differ mainly in the positioning of the α2 helix and the arrangement of β-strands β2–β4 (Fig. 3; Yoder *et al.*, 2001; Tilley *et al.*, 2004; Schouten *et al.*, 2002). Intuitively, when the lipid cargo phosphatidylinositol (PI) or phosphatidylcholine (PC) is bound, PITPα assumes the closed conformation (Fig. 3*a*; Yoder *et al.*, 2001; Tilley *et al.*, 2004). Also intuitively, at one point during the loading of PITPα with its lipid cargo, the protein must be in the unliganded state and be in the open conformation (Fig. 3*b*). Only then is the cavity accessible to solvent and poised for lipid exchange. This also means that microcolin drugs can only enter the cavity of the protein at the point of its lipid-exchange cycle. What is somewhat counterintuitive, however, is that after binding of microcolin H there is no closure of the cavity around the drug. Instead, PITPα remains in the open conformation in the microcolin-bound structure (Fig. 3*c*), which was also observed previously for PITPα in complex with the inhibitor VT01454 (Kim *et al.*, 2024).

Table 2
Pairwise r.m.s.d.s between PITPα structures bound to different ligands.

Root-mean-square deviations (r.m.s.d.s; Å) were calculated in *PyMOL* (beetween protein backbones with no outlier rejection) from structural superpositions of PITPα in the unliganded state and in complex with microcolin H, VT01454, phosphatidylcholine (PC) or phosphatidylinositol (PI). Structurally similar pairs are in green, whereas divergent pairs are in red.

	Unliganded	Microcolin H	VT01454	PC	PI
Unliganded	0	1.131	1.021	3.484	3.788
Microcolin H	1.131	0	0.478	3.088	3.377
VT01454	1.021	0.478	0	3.116	3.402
PC	3.484	3.088	3.116	0	0.962
PI	3.788	3.377	3.402	0.962	0

3.3. Analysis of PITPα cavities in the open and closed states

To quantify the differences between various ligand-bound states of PITPα, we calculated the pairwise root-mean-square deviations (r.m.s.d.s) between PITPα structures in the unliganded state and in complex with different ligands. The r.m.s.d. values reveal that PITPα bound to microcolin H or VT01454 is structurally similar to the unliganded protein, indicating that these ligands stabilize a comparable, open conformation. In contrast, substantially larger r.m.s.d.s are observed for comparisons involving PC- or PI-bound structures with unliganded PITPα, reflecting the distinct closed conformation adopted upon lipid binding. Together, these data highlight a clear structural separation between inhibitor-bound/open and lipid-bound/closed states of PITPα (Table 2).

Next, we analyzed the volumes of PITPα cavities. Unlike the volumes of regular Euclidean solids, the volume of a protein cavity is not well defined, and the numerical result strongly depends on the algorithm used for its calculation. Typically, such algorithms use a spherical probe of a given diameter, usually similar to that of a water molecule, and determine the positions within the protein structure that can be occupied by this probe. Although this approach is widely accepted, the resulting volume depends on the specific parameters and implementation of the program used. We employed *CavitOmiX*, a *PyMOL* plugin, as described in detail in Section 2. Using these settings, the calculated cavity volumes were 844 Å^3 for PI-bound PITPα (the only closed conformation), 2799 Å^3 for microcolin H-bound PITPα, 2728 Å^3 for unliganded mouse PITPα and 2346 Å^3 for VT01454-bound PITPα (Fig. 4). These results, obtained using an independent approach and without the need to directly observe conformational changes, illustrate that microcolin-bound PITPα adopts the open conformation.

Typical methods used to study protein–small-molecule interactions include isothermal titration calorimetry, surface plasmon resonance, fluorescence resonance energy transfer, fluorescence anisotropy and related techniques (Su & Xu, 2018; Sülzen *et al.*, 2025; Okamoto & Sako, 2017; Rezabkova *et al.*, 2010). These approaches provide binding constants and, in some cases, kinetic parameters or thermodynamic contributions such as enthalpy and entropy (Smola *et al.*, 2021). However, they do not reveal how a ligand interacts with its target protein at the atomic level. Instead, binding modes are often inferred using computational simulations based on a protein structure determined in an unliganded state or in

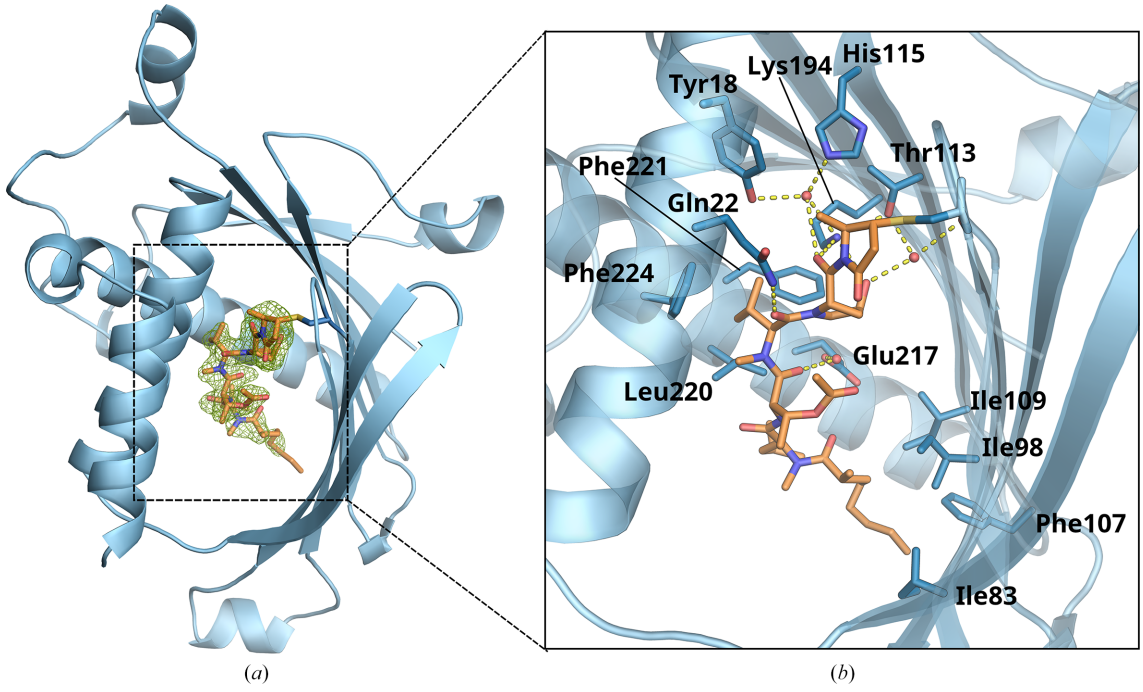

Figure 2
Crystal structure of the PITPα–microcolin H complex. (*a*) Overall structure of PITPα with bound microcolin H. Microcolin H is shown with its electron-density map ($F_o - F_c$ map) contoured at 3σ and colored green. (*b*) Close up-view of the interactions between PITPα and microcolin H. Microcolin H is depicted as orange sticks and PITPα is colored blue. Microcolin H-interacting residues are shown as dark blue sticks. Selected hydrogen bonds are indicated by yellow dashed lines and water molecules involved in water bridges are depicted as red spheres.

complex with a different ligand (Gazgalis *et al.*, 2020; Guterres *et al.*, 2019). If the protein structure used for modeling does not represent the conformation adopted during binding of the ligand of interest, the resulting simulation results will be highly inaccurate, at best. Our results highlight the importance of determining the correct protein conformation under ligand-bound conditions. Specifically, a docking experiment using the VT01454 inhibitor could not correctly predict the structure as it assumed that the PITP domain was in the closed conformation (Kim *et al.*, 2024). Similarly, a recent computational study (Bailly & Vergoten, 2025) used the PC-bound state of the PITP domain to predict microcolin binding to the protein *in silico* and therefore reached an inaccurate conclusion.

In summary, the structures reported here and in Kim *et al.* (2024) showing how microcolins target class I PITPs reveal that these inhibitors stabilize the open conformation of the protein. The importance of this finding is that it allows us to draw some conclusions regarding the functions of these proteins. Previous structural studies showed that class I PITPs are found in a closed conformation when they hold their lipid cargo (Yoder *et al.*, 2001; Tilley *et al.*, 2004). To exchange its lipid cargo, the protein must assume an open conformation that must be facilitated by its transient interaction with membranes. In fact, studies with mutant proteins truncated in their C-termini that interfere with closing on their cargo showed that such mutants show significantly stronger membrane binding (Grabon *et al.*, 2017; Schouten *et al.*, 2002). Based on these data, access of the inhibitor to the cargo bay of the proteins must take place at the point where the protein interacts with the membrane, *i.e.* when it presents its open

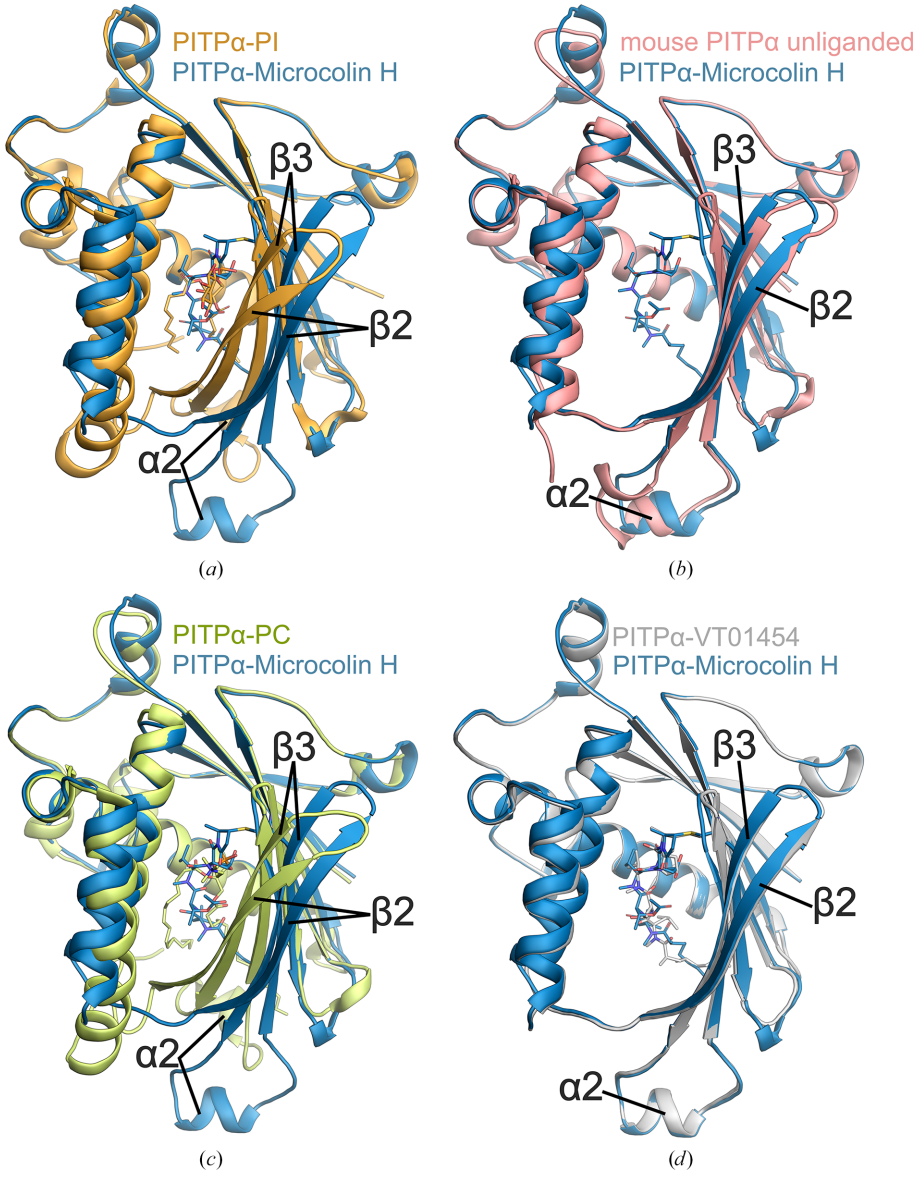

Figure 3
Structural comparison of the PITPα–microcolin H complex with previously reported PITPα structures. Structural alignment of the PITPα–microcolin H complex (blue) with (*a*) PI-bound PITPα (orange; PDB entry 1uw5), (*b*) mouse unliganded PITPα (pink; PDB entry 1kcm), (*c*) PC-bound PITPα (green; PDB entry 1t27) and (*d*) the PITPα–VT01454 complex (gray; PDB entry 8pqo).

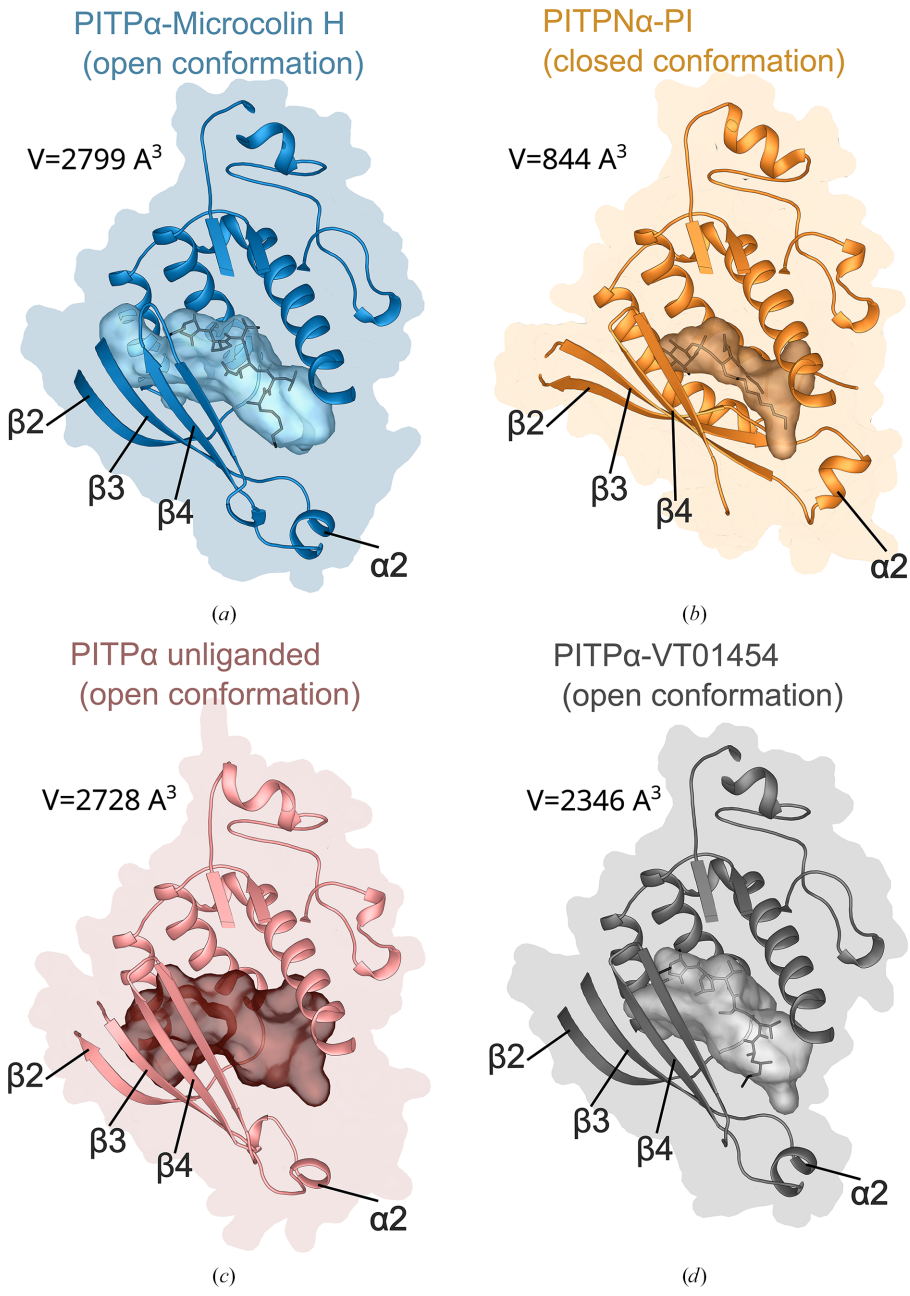

Figure 4
Binding cavities of PITPα in the microcolin H- and PI-bound states. The microcolin H complex is shown in blue (*a*). For comparison, the PI-bound PITPα structure is shown as a light-orange cartoon (*b*), unliganded PITP is in salmon (*c*) and VT01454-bound PITP is in gray (*d*). The cavity volume corresponds to the conformation of PITPα.

conformation (Schouten *et al.*, 2002). Our previous data showed that the treatment of cells expressing a GFP-tagged PITPα or PITPβ with the inhibitor VT01454 caused the otherwise cytoplasmic protein to associate with membranes (Kim *et al.*, 2024). This finding was consistent with the conclusion that even under the conditions of live cell experiments, the inhibitor replaces the lipid cargo when the PITP interacts with the membrane, and by stabilizing the open conformation it causes the protein to remain membrane-bound. It is important to note that without permanent binding, which takes place with these inhibitors, the open conformation and membrane interaction is extremely short-lived and transient, as previously suggested by molecular-dynamics simulation studies (Grabon *et al.*, 2017). The current results showing that another covalently bound inhibitor also promotes the open conformation gives further support to this model of structural transition during lipid exchange at the membrane.

Acknowledgements

We thank the Helmholtz-Zentrum Berlin für Materialien und Energie for the allocation of synchrotron-radiation beamtime. We would particularly like to acknowledge Frank Lennartz and Petr Pachl for help and support during the experiment.

Funding information

This research was supported by the project 'New Technologies for Translational Research in Pharmaceutical Sciences'/ NETPHARM, project ID CZ.02.01.01/00/22_008/0004607 (co-funded by the European Union).

References

Afonine, P. V., Grosse-Kunstleve, R. W., Echols, N., Headd, J. J., Moriarty, N. W., Mustyakimov, M., Terwilliger, T. C., Urzhumtsev, A., Zwart, P. H. & Adams, P. D. (2012). *Acta Cryst.* D**68**, 352–367.

Ashlin, T. G., Blunsom, N. J. & Cockcroft, S. (2021). *Biochim. Biophys. Acta*, **1866**, 158985.

Bailly, C. & Vergoten, G. (2025). *Future Pharmacol.* **5**, 13.

Eisenreichova, A., Humpolickova, J., Różycki, B., Boura, E. & Koukalova, A. (2023). *Biochimie*, **215**, 42–49.

Eisenreichova, A., Klima, M., Anila, M., Koukalova, A., Humpolickova, J., Różycki, B. & Boura, E. (2023). *Cells*, **12**, 1974.

Emsley, P., Lohkamp, B., Scott, W. G. & Cowtan, K. (2010). *Acta Cryst.* D**66**, 486–501.

Garner, K., Hunt, A. N., Koster, G., Somerharju, P., Groves, E., Li, M., Raghu, P., Holic, R. & Cockcroft, S. (2012). *J. Biol. Chem.* **287**, 32263–32276.

Gazgalis, D., Zaka, M., Abbasi, B. H., Logothetis, D. E., Mezei, M. & Cui, M. (2020). *ACS Omega*, **5**, 14297–14307.

Grabon, A., Bankaitis, V. A. & McDermott, M. I. (2019). *J. Lipid Res.* **60**, 242–268.

Grabon, A., Orłowski, A., Tripathi, A., Vuorio, J., Javanainen, M., Róg, T., Lönnfors, M., McDermott, M. I., Siebert, G., Somerharju, P., Vattulainen, I. & Bankaitis, V. A. (2017). *J. Biol. Chem.* **292**, 14438–14455.

Guterres, H., Lee, H. S. & Im, W. (2019). *J. Chem. Theory Comput.* **15**, 6524–6535.

Kabsch, W. (2010). *Acta Cryst.* D**66**, 125–132.

Kim, D., Lee, S., Jun, Y. & Lee, C. (2025). *Proc. Natl Acad. Sci. USA*, **122**, e2516849122.

Kim, Y. J., Pemberton, J. G., Eisenreichova, A., Mandal, A., Koukalova, A., Rohilla, P., Sohn, M., Konradi, A. W., Tang, T. T., Boura, E. & Balla, T. (2024). *EMBO J.* **43**, 2035–2061.

Li, F. L., Fu, V., Liu, G. B., Tang, T., Konradi, A. W., Peng, X., Kemper, E., Cravatt, B. F., Franklin, J. M., Wu, Z. M., Mayfield, J., Dixon, J. E., Gerwick, W. H. & Guan, K. L. (2022). *Nat. Chem. Biol.* **18**, 1076–1086.

Liebschner, D., Afonine, P. V., Baker, M. L., Bunkóczi, G., Chen, V. B., Croll, T. I., Hintze, B., Hung, L.-W., Jain, S., McCoy, A. J., Moriarty, N. W., Oeffner, R. D., Poon, B. K., Prisant, M. G., Read, R. J., Richardson, J. S., Richardson, D. C., Sammito, M. D., Sobolev, O. V., Stockwell, D. H., Terwilliger, T. C., Urzhumtsev, A. G., Videau, L. L., Williams, C. J. & Adams, P. D. (2019). *Acta Cryst.* D**75**, 861–877.

McCoy, A. J., Grosse-Kunstleve, R. W., Adams, P. D., Winn, M. D., Storoni, L. C. & Read, R. J. (2007). *J. Appl. Cryst.* **40**, 658–674.

Mueller, U., Barthel, T., Benz, L. S., Bon, V., Crosskey, T., Genter Dieguez, C., Förster, R., Gless, C., Hauss, T., Heinemann, U., Hellmig, M., James, D., Lennartz, F., Oelker, M., Ovsyannikov, R., Singh, P., Wahl, M. C., Weber, G. & Weiss, M. S. (2025). *J. Synchrotron Rad.* **32**, 766–778.

Okamoto, K. & Sako, Y. (2017). *Curr. Opin. Struct. Biol.* **46**, 16–23.

Pathak, A., Willis, K. G., Bankaitis, V. A. & McDermott, M. I. (2024). *Biochim. Biophys. Acta*, **1869**, 159529.

Raghu, P., Basak, B. & Krishnan, H. (2021). *Biochim. Biophys. Acta*, **1866**, 158984.

Rezabkova, L., Boura, E., Herman, P., Vecer, J., Bourova, L., Sulc, M., Svoboda, P., Obsilova, V. & Obsil, T. (2010). *J. Struct. Biol.* **170**, 451–461.

Schouten, A., Agianian, B., Westerman, J., Kroon, J., Wirtz, K. W. A. & Gros, P. (2002). *EMBO J.* **21**, 2117–2121.

Smola, M., Gutten, O., Dejmek, M., Kožíšek, M., Evangelidis, T., Tehrani, Z. A., Novotná, B., Nencka, R., Birkuš, G., Rulíšek, L. & Boura, E. (2021). *Angew. Chem. Int. Ed.* **60**, 10172–10178.

Sparta, K. M., Krug, M., Heinemann, U., Mueller, U. & Weiss, M. S. (2016). *J. Appl. Cryst.* **49**, 1085–1092.

Su, H. & Xu, Y. (2018). *Front. Pharmacol.* **9**, 1133.

Sülzen, H., Klima, M., Duchoslav, V. & Boura, E. (2025). *Biophys. Chem.* **319**, 107392.

Tilley, S. J., Skippen, A., Murray-Rust, J., Swigart, P. M., Stewart, A., Morgan, C. P., Cockcroft, S. & McDonald, N. Q. (2004). *Structure*, **12**, 317–326.

Wirtz, K. W. & Zilversmit, D. B. (1969). *Biochim. Biophys. Acta*, **193**, 105–116.

Yang, H., Zhang, X., Wang, C., Zhang, H., Yi, J., Wang, K., Hou, Y., Ji, P., Jin, X., Li, C., Zhang, M., Huang, S., Jia, H., Hu, K., Mou, L. & Wang, R. (2023). *Signal Transduct. Target. Ther.* **8**, 428.

Yoder, M. D., Thomas, L. M., Tremblay, J. M., Oliver, R. L., Yarbrough, L. R. & Helmkamp, G. J. (2001). *J. Biol. Chem.* **276**, 9246–9252.

Zhang, J. (2025). *Mar. Drugs*, **23**, 283.